https://doi.org/10.5194/bg-2022-82
Preprint. Discussion started: 30 March 2022

Biogeosciences Discussions

On physical mechanisms controlling air–sea CO_2 exchange

Lucía Gutiérrez-Loza[1], Erik Nilsson[1], Marcus B. Wallin[1,2], Erik Sahlée[1], and Anna Rutgersson[1]

[1]Department of Earth Sciences, Uppsala University, Uppsala, Sweden
[2]Department of Aquatic Sciences and Assessment, Swedish University of agricultural Sciences, Uppsala, Sweden

Correspondence: Lucía Gutiérrez-Loza (lucia.gutierrez_loza@geo.uu.se)

Abstract.

Reducing uncertainties in the air–sea CO_2 flux calculations is one of the major challenges when addressing the oceanic contribution in the global carbon balance. In traditional models, the air–sea CO_2 flux is estimated using expressions of the gas transfer velocity as a function of wind speed. However, other mechanisms affecting the variability in the flux at local and regional scales are still poorly understood. The uncertainties associated with the flux estimates become particularly large in heterogeneous environments such as coastal and marginal seas. Here, we investigated the air–sea CO_2 exchange at a coastal site in the central Baltic Sea using nine years of eddy covariance measurements. To the best of our knowledge, this is the longest record of direct observations of CO_2 fluxes and the corresponding gas transfer velocities (k) in a marine environment. Based on these observations we were able to capture the temporal variability of the air–sea CO_2 flux and other parameters relevant for the gas exchange. The analysis of water-side and atmospheric control mechanisms showed that during wind speeds above $8\,\mathrm{m\,s^{-1}}$ the conditions on both sides of the air–water interface were relevant for the gas exchange. Our findings further suggest that at such relatively high wind speeds, sea spray was an efficient mechanisms for air–sea CO_2 exchange. In contrast to high wind-speed conditions, during low wind speeds (<$6\,\mathrm{m\,s^{-1}}$) only water-side processes were found to be relevant control mechanisms, in particular, water-side convective processes. Altogether, our results show that currently existing wind-based parametrizations of k might be good approximations as long-term averages for environments with coastal characteristics. However, in order to reduce the uncertainty associated to these averages and produce reliable short-term k estimates, additional physical processes must be considered.

1 Introduction

Air–sea CO_2 exchange is an essential aspect of the global carbon cycle, having great implications for the Earth's climate. The global oceans are estimated to be net sinks of CO_2 taking up on average ca 25 % of the CO_2 emitted every year to the atmosphere due to anthropogenic activities (Friedlingstein et al., 2021). The current global ocean uptake is estimated to be between -2.0 and -3.1 $\mathrm{GtC\,yr^{-1}}$ (Takahashi et al., 2009; Ciais et al., 2013; Friedlingstein et al., 2021). However, large uncertainties are still associated with the air–sea CO_2 flux estimates, mainly due to the incomplete understanding of the spatio-temporal variability in the controlling mechanisms.

https://doi.org/10.5194/bg-2022-82
Preprint. Discussion started: 30 March 2022

Biogeosciences Discussions Open Access EGU

The exchange of CO_2 across the air–sea interface can be described using the following bulk formula:

$$FCO_2 = kK_0 \Delta pCO_2 = kK_0(pCO_2^w - pCO_2^a), \quad (1)$$

where the air–sea CO_2 flux (FCO_2) is a function of the gas transfer velocity (k), the difference in the partial pressure of CO_2 (ΔpCO_2) between the atmosphere and the seawater (superscripts a and w, respectively), and the salinity- and temperature-dependent solubility constant (K_0). The direction of the flux is determined by the sign of ΔpCO_2 and, by convention, positive (upward) FCO_2 represents transport from the ocean to the atmosphere (i.e. positive ΔpCO_2).

The gas transfer velocity, k, represents the efficiency of the transfer processes across the air–sea interface. For CO_2 and other slightly soluble gases, such efficiency is particularly associated to the turbulent processes occurring in the oceanic boundary layer, which ultimately control the air–sea gas exchange. The wind can be associated, directly or indirectly, with most of the turbulent process near the ocean–atmosphere interface. Thus, the traditional approach suggests that k can be represented as a function of the the wind speed since it is the largest source of kinetic energy to the upper ocean. With wind-speed data being a widely available resource globally, wind-based parametrizations of k have often been used to obtain global estimates of FCO_2 (e.g. Takahashi et al., 2009). However, large uncertainties in the estimated FCO_2 have been associated to the uncertainties in k (Woolf et al., 2019). At regional and local scales, the magnitude of these uncertainties becomes especially problematic, particularly in coastal environments where adequate representation of the physical and biogeochemical processes, and their interactions, is necessary in order to avoid large biases in the flux estimates.

In addition to the wind speed, other water-side control mechanisms are well known to play a significant role in the gas transfer processes of slightly soluble gases, such as CO_2. Furthermore, the effect of atmospheric controls, and their impact on the upper layer of the ocean, are potentially relevant (e.g. Erickson III, 1993) but seldom considered. The relative importance of these forcing mechanisms on the gas exchange is highly dependent on the characteristics near the sea surface, which in turn, can be categorized based on wind-speed regimes (e.g. Soloviev and Lukas, 2013). At moderately high wind speeds, above 8–10 $\mathrm{m\,s^{-1}}$, the upper layer of the ocean is generally well mixed. Under these conditions, breaking waves (Zhao et al., 2003; Blomquist et al., 2017; Brumer et al., 2017), bubbles (Woolf, 1993, 1997; Bell et al., 2017), and sea spray (Andreas et al., 2016) have a significant role on air–sea interaction processes. At wind speeds lower than 4–5 $\mathrm{m\,s^{-1}}$, when the effects of breaking waves and wind-induced mixing are limited, convective processes in the atmosphere (Erickson III, 1993) and the sea (Rutgersson and Smedman, 2010) become relevant. Other processes such as surface films (Pereira et al., 2018; Ribas-Ribas et al., 2018), rain (Ashton et al., 2016), Langmuir circulation (Thorpe et al., 2003), and micro-scale wave breaking (Jessup et al., 1997) might be relevant over a wider range of wind speeds, including intermediate wind velocities. In order to explain the variability and reduce the uncertainty in FCO_2 estimates, it is necessary to understand the effect of the control mechanisms on gas exchange, particularly at higher wind speeds but even relevant at low and moderate wind speeds.

Coastal oceans and marginal seas are active and heterogeneous environments in terms of both physical and biogeochemical processes. These regions have been found to be net sinks of CO_2 at global scales (Borges et al., 2005; Laruelle et al., 2010; Chen et al., 2013) with disproportionately large contributions to the global carbon system when compared to the open ocean

https://doi.org/10.5194/bg-2022-82
Preprint. Discussion started: 30 March 2022

(Laruelle et al., 2014). The complexity and heterogeneity of the coastal regions causes large spatio-temporal variability in the air–sea CO_2 exchange (Roobaert et al., 2019), variability that is rarely accounted for in global estimates.

The Baltic Sea is a semi-enclosed sea located at relatively high latitudes, stretching from 54° N to 66° N. The basin is largely affected by terrestrial inputs from surrounding watersheds and has relatively limited water exchange with the open ocean. This leads to a dynamic carbon system with significant spatio-temporal variability. In terms of the air–sea CO_2 exchange, several approaches have been used to estimate the regional fluxes, however, no consensus has been reached on the role of the Baltic Sea as a net source or sink of atmospheric CO_2 (Thomas et al., 2010; Kuliński and Pempkowiak, 2011; Norman et al., 2013b; Parard et al., 2017). In order to resolve some of the key elements associated to the air–sea CO_2 exchange, previous studies have focused on the diurnal (Honkanen et al., 2021) and seasonal (Thomas and Schneider, 1999; Rutgersson et al., 2008; Schneider et al., 2014) variability in the partial pressure of CO_2 across the Baltic Sea, and on the spatial and temporal variability in the atmospheric CO_2 concentrations (Rutgersson et al., 2009). Furthermore, water-side convection (Rutgersson and Smedman, 2010; Norman et al., 2013b), upwelling events (Norman et al., 2013a; Jacobs et al., 2021), and ice coverage (Löffler et al., 2012) have all been recognized as important regional controls on the gas exchange. Despite these efforts, the effect of the different mechanisms modulating the air–sea gas exchange, and its variability, is still poorly understood in the Baltic Sea, as it is in many other coastal regions. Limited data availability is the main reason hindering our ability to resolve processes at relevant spatial and temporal scales. In this context, continuous and long-term monitoring of the air–sea CO_2 exchange in coastal areas is essential to improve our understanding of the gas transfer mechanisms.

In this study, we present and evaluate data collected during a nine-year period at the land-based station Östergarnsholm located on an island in the central Baltic Sea. This is, to the best of our knowledge, the longest record of air–sea CO_2 flux based on eddy covariance measurements. Using atmospheric and water-side data we evaluated different control mechanisms modulating the gas transfer velocity, k, covering a wide range of wind speed conditions.

2 Site and Data

2.1 The Östergarnsholm site

We used data collected between 2013 and 2021 from the Swedish marine Integrated Carbon Observation System (ICOS) station, Östergarnsholm. The station (57° 27' N, 18° 59' E) is located on a small and flat island located 4 km east of the bigger island of Gotland in the central Baltic Sea (Fig. 1). Measurements are performed in a 30 m land-based tower located on the southern tip of the island, with the base of the tower at 1.4 m above the mean sea level (Sjöblom and Smedman, 2002). The tower has been used to monitor and study the marine atmospheric boundary layer and air–sea interaction processes since 1995 (e.g. Smedman et al., 1999; Rutgersson et al., 2001; Högström et al., 2008; Rutgersson and Smedman, 2010; Rutgersson et al., 2020).

https://doi.org/10.5194/bg-2022-82
Preprint. Discussion started: 30 March 2022

Biogeosciences
Discussions
Open Access
EGU

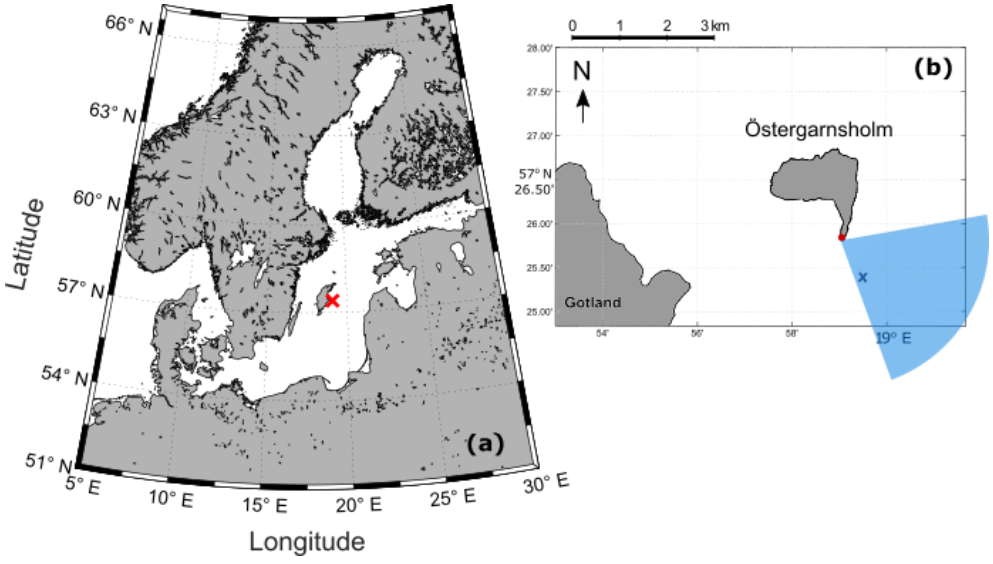

Figure 1. (a) Map of the Baltic Sea; the red cross in the central Baltic Sea indicates the location of the Östergarnsholm station. (b) Map of the Östergarnsholm station ca 4 km off from the Gotland Island; the red dot indicates the location of the tower, the blue cross is the location of the mooring with water-side instrumentation (Sect. 2.1.2), and the shaded blue area is the so-called "open-sea" sector (see text for details).

2.1.1 Atmospheric data

The tower at Östergarnsholm was instrumented with high-frequency sensors for continuous turbulence measurements. CO_2 fluxes were calculated using the fluctuations of the vertical wind component measured by a CSAT3-3D sonic anemometer (Campbell Scientific, Inc., Logan, UT, USA) and the fluctuations of the atmospheric CO_2 molar densities measured with a LI-7500 open-path gas analyzer (LI-COR, Inc., Lincoln, NE, USA). For details about the flux calculations see Sect. 2.2. Both instruments were located at a height of 9 m from the tower base and sampled at a rate of 20 Hz. In addition to the high-frequency data, profile measurements of wind speed, wind direction, and temperature at 7, 12, 14, 20, and 29 m height were carried out at 1 Hz and averaged over 30 min periods. Relative humidity, atmospheric pressure, incoming solar radiation, and precipitation were also measured at the site.

The measurements at the Östergarnsholm site have been found to be representative of open-sea or coastal conditions depending on the wind direction (Rutgersson et al., 2020). Only data with wind directions from southeast ($80° < WD < 160°$) representing open-sea conditions were included in the analysis of the current study (Fig. 1b). For this wind sector, it was considered that no disturbances occurred in the tower measurements due to flow distortion, and that the wave field was not affected by the shallowing of the seafloor (Högström et al., 2008). Furthermore, the biogeochemical water properties were assumed to be homogeneous for this sector (Rutgersson et al., 2008). A more detailed description of the Östergarnsholm site can be found in Rutgersson et al. (2020).

https://doi.org/10.5194/bg-2022-82
Preprint. Discussion started: 30 March 2022

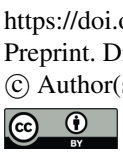

Biogeosciences Discussions Open Access EGU

According to the flux footprint estimates (Kljun et al., 2015), the source/sink area of the fluxes from the open-sea sector was located a few hundred meters upwind from the tower (Fig. 2). For unstable and neutral conditions, the main flux source/sink was found as a localized area near the tower. While for stable conditions, the source/sink contributions per unit area were smaller closer to the tower and rather spread over a larger region.

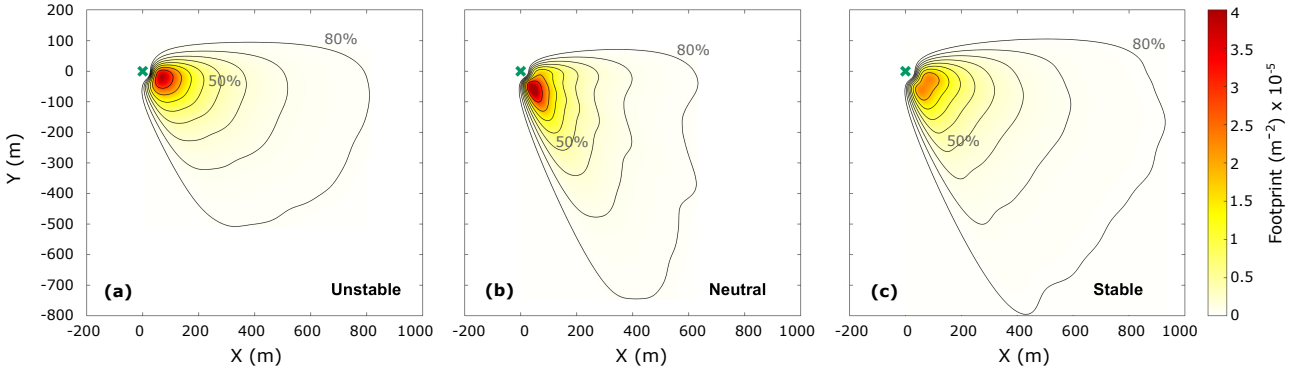

Figure 2. Average footprint distribution for (a) unstable, (b) neutral, and (c) stable atmospheric conditions. The green cross indicates the position of the tower and the contours represent the percentage of source area from 10–80 %. The flux footprint was calculated using the model developed by Kljun et al. (2015) using all data available for the open-sea sector between mid-2013 and 2020.

The atmospheric stability was represented as z/L, where z is the measurement height and L is the Monin-Obukhov length. The latter is given by $L = -u_*^3\Theta/g\kappa\overline{w'T_s'}$, where u_* is the friction velocity, Θ is the potential temperature, $g = 9.81\ \mathrm{m\,s^{-2}}$ is the acceleration due to gravity, $\kappa = 0.4$ is the Von Karman constant, and $\overline{w'T_s'}$ is the buoyancy flux. The sonic temperature, T_s, was considered to be almost equal to the virtual temperature, T_v, which is often used for buoyancy flux calculations (Aubinet et al., 2012). Following Sjöblom and Smedman (2002), we use $z = 10.4\ \mathrm{m}$ as the mean measurement height with respect to the mean sea level. Here, unstable conditions were defined as $z/L \leq$ -0.05, near-neutral conditions -0.05 $< z/L <$ 0.05, and stable conditions $z/L \geq$ 0.05.

2.1.2 Water-side measurements

Water-side measurements were carried out continuously at a mooring located 1 km southeast of the tower (see Fig.1b). At the mooring, seawater temperature and partial pressure of CO_2 were measured every 30 min using a SAMI-CO_2 sensor (Sunburst Sensors, LLC, MT, USA) at a depth of 4 m. Additionally, continuous wave measurements were made with a Directional Waverider buoy located 4 km southeast of the tower (outside the domain in Fig. 1b). The Waverider buoy is operated and maintained by the Finnish Meteorological Institute (FMI). In this study, the characteristics of the sea state were represented by the significant wave height (H_s), the wave steepness calculated as H_s/L_p were L_p is the peak wavelength, and the wave age, C_p/U_{10N}, were C_p is the phase velocity of the waves and U_{10N} is the neutral equivalent wind speed at 10 m height.

https://doi.org/10.5194/bg-2022-82
Preprint. Discussion started: 30 March 2022

Daily data of the mixed layer depth (MLD) from the Baltic Sea Reanalysis product provided by the Copernicus Marine Environment Monitoring System (CMEMS) (Von Schuckmann et al., 2016) were used as an indicator of the vertical mixing in the water column, and for the water-side convection calculations (Rutgersson and Smedman, 2010; Norman et al., 2013b). These data are freely available from CMEMS website at http://marine.copernicus.eu/services-portfolio/access-to-products/.

2.2 Data processing

High frequency data obtained at Östergarnsholm site (Sect. 2.1.1) were used for FCO_2 calculations using the eddy covariance method (Baldocchi et al., 1988; Aubinet et al., 2012) and the subsequent gas transfer velocity analysis. The turbulent fluctuations for the flux calculation (described below) were obtained following a Reynolds decomposition using an average period of 10 min. These averages were calculated as block averages from the linearly detrended time series of the 20 Hz data. The turbulent fluctuations were used to calculate variances and covariances. Other statistical moments were also calculated from the turbulent fluctuations and used as part of the quality control.

The raw wind-speed components were transformed to earth-system coordinates and corrected using a double rotation (Kaimal and Finnigan, 1994). Wind speed and direction were calculated from the corrected components to avoid effects caused by the tilting of the sonic anemometer. Following the convention, measured wind speeds were adjusted to a neutral equivalent wind speed at 10 m height (U_{10N}). Only wind directions representing open-sea conditions were used in the analysis; see Sect. 2.1.1 for details. Only periods with the three consecutive 10 min averages from 80 ° < WD < 160 ° (i.e. open-sea sector) were included. Data with wind speeds lower than 2 $\mathrm{m\,s^{-1}}$ was excluded for the FCO_2 calculations.

The performance of the gas analyzer was evaluated based on the relative signal strength indicator (RSSI). Following Nilsson et al. (2018), we used the variance of the RSSI (σ^2_{RSSI}) to remove low quality data. The variance was calculated over the 10 min periods, and only data with $\sigma^2_{RSSI} < 0.001$ were considered in the analysis. Additionally, thresholds of different statistical parameters were used to ensure the homogeneity of the data and avoid outliers. Data was excluded if the absolute value of the fourth order moment of the CO_2 signal was higher than 100 $\mathrm{ppm^4}$ to filter out outliers, and the variance of the vertical wind speed was $\sigma^2_w < 1e^{-6}\,\mathrm{m^2\,s^{-2}}$ to exclude unrealistically low values of the vertical wind variance.

According to the eddy covariance method, the FCO_2 were calculated from:

$$FCO_2 = \rho_a \overline{w'c'}, \tag{2}$$

where, ρ_a is the mean density of dry air, and the term $\overline{w'c'}$ represents the time-averaged covariance between the turbulent fluctuations of the vertical wind component (w) and the dry mole fraction of the gas (c). The FCO_2 were calculated over 30 min periods by averaging three consecutive 10 min periods fulfilling all the quality-control steps. The flux was directly calculated from the CO_2 dry mole fraction (i.e. mole fraction of CO_2 relative to dry air) obtained from the measured molar densities of CO_2 relative to the ambient air. By using this direct conversion method (Sahlée et al., 2008), the corrections for dilution effects (Webb et al., 1980) were avoided. A description of the direct conversion method and detailed discussion can be found in Sahlée et al. (2008). Fluxes with magnitudes below a minimum detection limit of $\pm 0.05\,\mathrm{\mu mol\,m^{-2}\,s^{-1}}$ were removed.

https://doi.org/10.5194/bg-2022-82
Preprint. Discussion started: 30 March 2022


Biogeosciences Discussions Open Access EGU

This limit was empirically defined to avoid data with low signal-to-noise ratio. In addition to FCO_2, enthalpy fluxes were also estimated from the turbulent measurements as the sum of the sensible ($\rho C_p \overline{w'T'}$) and latent ($\rho\lambda\overline{w'q'}$) heat fluxes. Furthermore, cases with high relative humidity conditions (RH$>$ 95 %) were excluded to avoid data possibly affected by condensation on the instruments.

The gas transfer velocity was calculated from Eq. 1 using the calculated FCO_2 (Eq. 2). The solubility constant (K_0) was determined from the relationship suggested by Weiss (1974) using a constant salinity value of 7 PSU and in situ water temperature from the SAMI sensor. Changes in the salinity, which oscillates between 6.5 and 7.5 PSU in these region of the Baltic, are not expected to have significant effects on the solubility in comparison to the effect of the water temperature variability. The ΔpCO_2 was obtained from pCO_2^w measured with the SAMI sensor, and pCO_2^a calculated from the molar densities obtained with the gas analyzer. A normalized gas transfer velocity (k_{660}) was calculated as $k_{660} = k(660/Sc)^{-1/2}$, where the reference, $Sc = 660$, corresponded to the Schmidt number of CO_2 at 20 °C for seawater (S = 35 ‰), and Sc was the Schmidt number calculated with the corresponding in situ water temperature (T_w) for each data point. Periods with $\Delta pCO_2 < \pm 50\,\mu\mathrm{atm}$ were excluded from the analysis. Furthermore, during conditions of strong water-side stratification, pCO_2^w measurements carried out at 4 m depth might not be representative of the air–sea CO_2 fluxes measured at the tower. Therefore, all the data occurring during strongly stratified conditions according to the in situ observations were not considered in the analysis. Data were removed when the water-side temperature gradient (ΔT_w) was larger than 1 °C. The ΔT_w was defined as the difference between T_w measured at 4 m depth and the near-surface water temperature (T_{ns}) measured at 0.35 m depth with the Waverider buoy. Finally, scattered negative k_{660} were expected due to the stochastic behaviour of turbulence. However, more negative k_{660} values than what can be explained by this inherent property of eddy covariance data were observed. There was no methodological reason to exclude such data from the data set as they fulfilled all previous quality control steps. Nonetheless, they were not used for the more detail analysis presented in Sect. 3.2.1 to Sect. 3.2.3, due to the lack of a viable physical explanation.

The calculated k_{660} were used to study the effect of water-side and atmospheric control mechanisms on air–sea CO_2 exchange. In order to remove the wind-speed dependency from k_{660}, a "residual" gas transfer velocity was calculated (k_r). This residual term was calculated for each half-hourly value as the difference between k_{660} and the wind-based parametrization from Wanninkhof (2014) (hereafter referred to as k_{W14}). For the analysis, the data were divided into three different wind-speed regimes from light breeze to moderate gale. The thresholds for these regimes were chosen depending on the expected conditions at the sea surface according to the Beaufort Scale (Barua, 2005). Low wind speeds were defined as $U_{10N} < 6\,\mathrm{m\,s^{-1}}$, covering conditions of light to moderate breeze; only ripples and small waves causing little disturbance on the surface were expected under these conditions. Intermediate conditions representing moderate breezes included wind speeds of $6 > U_{10N} < 8\,\mathrm{m\,s^{-1}}$. Finally, relatively high wind-speed conditions were defined as $U_{10N} > 8\,\mathrm{m\,s^{-1}}$ when moderate to long waves were expected, whitecaps and sea spray were likely to be observed; these wind speeds correspond to fresh breeze to moderate gale.

https://doi.org/10.5194/bg-2022-82
Preprint. Discussion started: 30 March 2022

3 Results

3.1 Oceanic and meteorological conditions: the annual cycle

The annual cycle, obtained using the nine years of data (2013–2021), showed a seasonal pattern in both pCO_2^w and pCO_2^a (Fig. 3a). The pCO_2^a variability was small, at least when compared to the variability in pCO_2^w. The lowest pCO_2^a were observed during the late summer and autumn with values often below 380 µatm. Higher values occurred during winter, reaching 440 µatm. While the monthly means of pCO_2^a oscillated around 410 µatm. An increasing trend in pCO_2^a was observed during the study period (not shown); a linear regression using the monthly averages suggested an increase of 0.2 ppm per month which corresponds to a total increase of approximately 20 ppm during the nine-year period. Both the trend and the seasonal variability in pCO_2^a were masked by the variability in pCO_2^w (Fig.3a). A strong seasonal pattern was observed for pCO_2^w with values higher than those in the atmosphere during the winter, and lower during summer. The lowest pCO_2^w reached values below 100 µatm during the summer of 2018. The highest values of pCO_2^w occurred during the winters of 2018–2019 and 2019–2020 with observed values higher than 800 µatm. Furthermore, lower summer pCO_2^w values were observed in the last three years in comparison to previous years. In this way, the inter-annual variability of pCO_2^w was mostly noticeable in terms of an increasing amplitude of the seasonal cycle during the last years.

The monthly means of FCO_2 showed a seasonal cycle with positive fluxes during the winter and negative during the summer (Fig. 3b). This seasonal pattern in the flux was consistent with the thermodynamic forcing (i.e. $\Delta pCO_2 = pCO_2^w - pCO_2^a$) which suggested an upward transport during the winter and downward during the summer. However, a high variability in the half-hourly data was observed year-round.

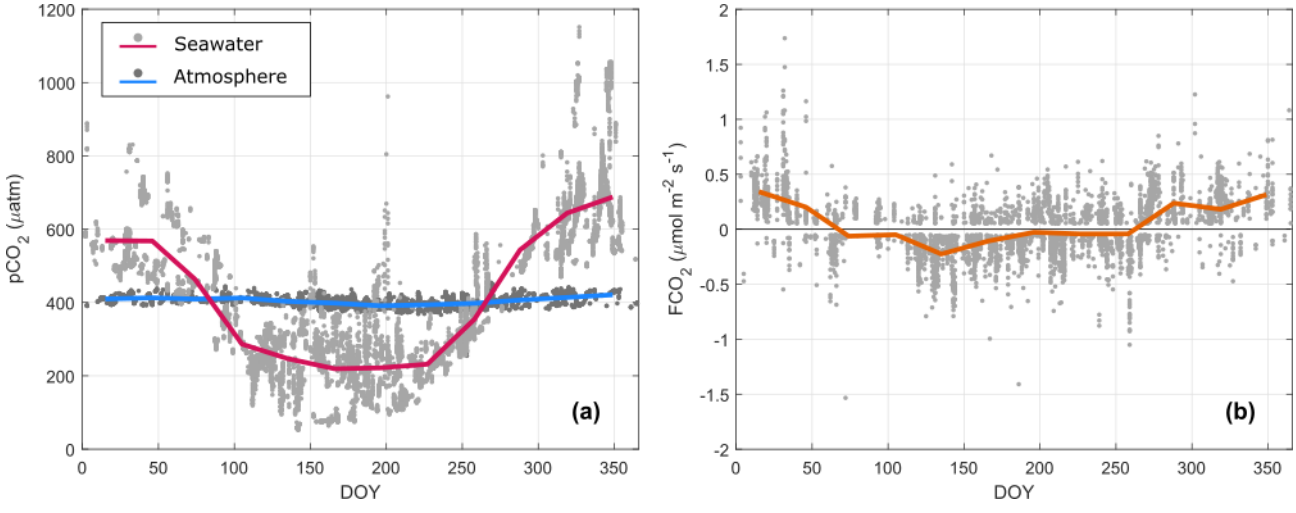

Figure 3. Annual cycle of (a) CO_2 partial pressure (pCO_2) in the seawater and in the atmosphere, and (b) air–sea CO_2 fluxes. The dots represent the half-hourly values while the solid lines show the monthly averages.

https://doi.org/10.5194/bg-2022-82
Preprint. Discussion started: 30 March 2022


Biogeosciences Discussions Open Access EGU

The atmospheric and water-side variables describing the physical characteristics showed clear seasonal cycles (Fig. 4). However, a large scatter was observed from the individual half-hourly values, thus, highlighting the large variability and heterogeneity of the environment. The monthly means of wind speed and significant wave height (H_s) were higher during the autumn and winter, in comparison to the summer (Fig. 4a and 4b). However, short-term events with high winds (U_{10N}>10 $\mathrm{m\,s^{-1}}$) and waves (H_s ~3 m) were observed during all seasons. The temperature gradient ($\Delta T = T_w - T_a$, Fig. 4c) showed that from September to February (DOY 250–50) the ocean was, on average, 1.5 °C warmer than the overlying air (i.e. positive gradient). During late spring, the atmospheric temperature was warmer than the seawater with an average ΔT of -1 °C. The enthalpy flux showed mean monthly values of 0–75 $\mathrm{W\,m^{-2}}$ (Fig. 4d). The monthly means of relative humidity (RH, Fig. 4e), ranged between 60 and 85 % throughout the year, but a large scatter was observed. Particularly during autumn and winter (DOY 250–50), when moderately low values of RH (<40 %) often occurred.

3.2 The gas transfer velocity

The normalized gas transfer velocity, k_{660}, followed a clear increasing relationship with wind speed (Fig. 5). At low and moderate wind speeds (up to ca 10 $\mathrm{m\,s^{-1}}$), the bin-averaged values of k_{660} followed commonly-used parametrizations. However, at wind speeds higher than 10 $\mathrm{m\,s^{-1}}$, the wind-speed dependency was more pronounced than the quadratic (Wanninkhof, 2014) and cubic (McGillis et al., 2001) relationships. Although the bin-averaged k_{660} values were generally in agreement with published parametrizations, we observed a large scatter in the half-hourly values along the entire wind-speed range. To further assess this variability in k_{660}, we evaluated atmospheric and water-side controls involved in the gas exchange under relatively high (Sect. 3.2.1), low (Sect. 3.2.2), and intermediate (Sect. 3.2.3) wind-speed conditions. For the description of the wind-speed regimes used in the following analysis see Sect. 2.2.

3.2.1 Controls on k_{660} at high wind speed conditions

At high wind speed conditions, the characteristics of the wave field (Fig. 6) were found to be associated to the gas exchange. The residual gas transfer velocity, k_r, showed a clear relationship with the significant wave height (H_s) as the highest values of k_r occurred during high-wave conditions of H_s>1.5 m (Fig. 6a). Low values of wave steepness (H_s/L_p) were observed even at the highest wind speeds with maximum values of 0.06 (Fig. 6b), much lower than the theoretical wave breaking threshold (Stokes, 1880). While the wave age (C_p/U_{10N}, Fig. 6c) suggests that most of the waves were locally generated (i.e. wind sea) at these wind speed conditions.

In addition to the wave field, we found ΔpCO_2 and MLD to be relevant water-side parameters which were associated to the behaviour of the gas transfer velocity (Fig. 7). Note that ΔpCO_2 was considered here as a water-side control due to the importance of pCO_2^w in modulating the variability of the gradient, in comparison to the rather constant values of pCO_2^a (see Sect. 3.1). Under conditions of strong gradients, where the absolute magnitude of ΔpCO_2 was higher than 200 μatm, k_{660} followed the wind-based parametrization ($k_r \approx 0$). Nonetheless, the largest values of k_{660} were not related to such strong gradients, instead, they were related to moderate positive ΔpCO_2 values in the order of 50-100 μatm (Fig. 7a). Large negative values of ΔpCO_2 were, in most cases, linked to negative values of k_r, thus, lower-than-expected from the wind-

https://doi.org/10.5194/bg-2022-82
Preprint. Discussion started: 30 March 2022

Biogeosciences
Discussions
Open Access
EGU

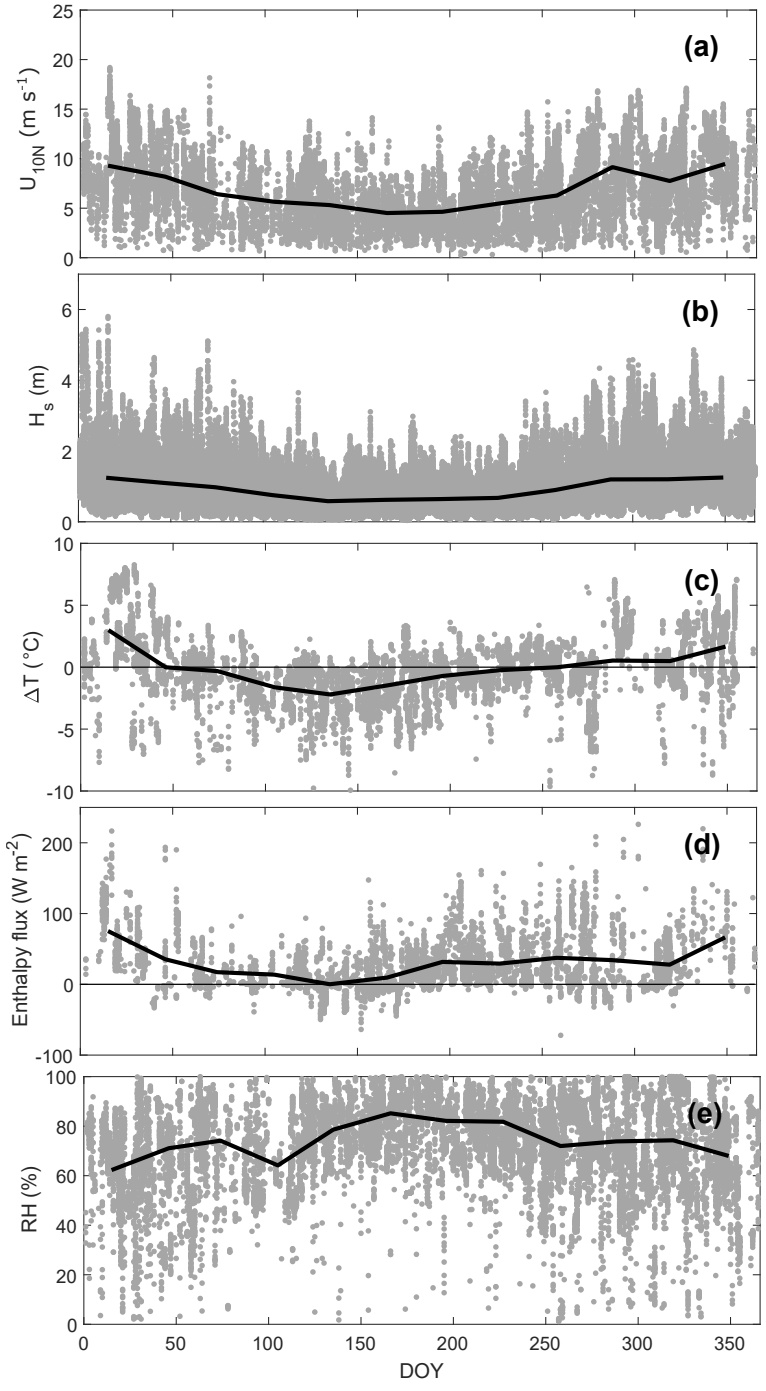

Figure 4. Annual cycle of (a) 10 m neutral wind speed, (b) significant wave height, (c) temperature gradient ($\Delta T = T_w - T_a$), (d) enthalpy flux, and (e) relative humidity. The dots are the half-hourly values while the solid black lines represent the monthly average of each parameter.

https://doi.org/10.5194/bg-2022-82
Preprint. Discussion started: 30 March 2022

Biogeosciences Discussions
Open Access
EGU

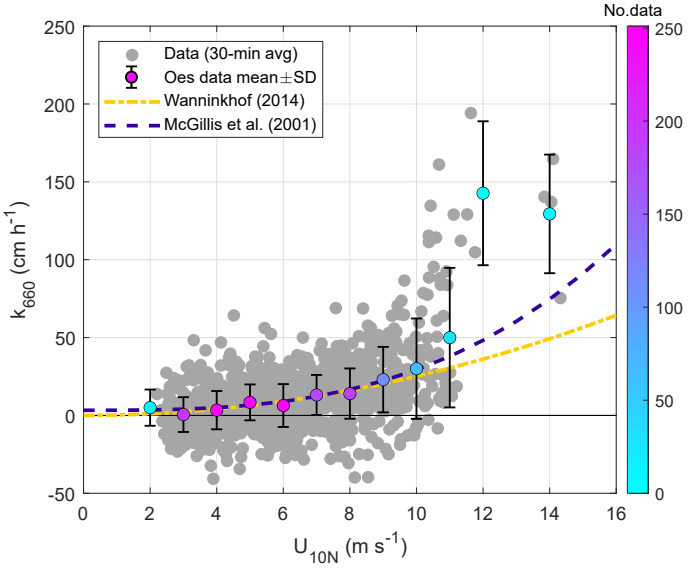

Figure 5. Gas transfer velocity for CO_2 (normalized to a Schmidt number of 660) as a function of the 10 m neutral wind speed. For reference, a quadratic (Wanninkhof, 2014) and cubic (McGillis et al., 2001) wind-based parametrizations were included. The grey dots represent the half-hourly values, the colored circles with bars represent the averages over $1\,\mathrm{m\,s^{-1}}$ bins and $\pm 1\sigma$. The colorbar indicates the amount of data (No. data) available per bin. The calculations of k_{660} were based on the data retrieved during the nine-year period from 2013 to 2021.

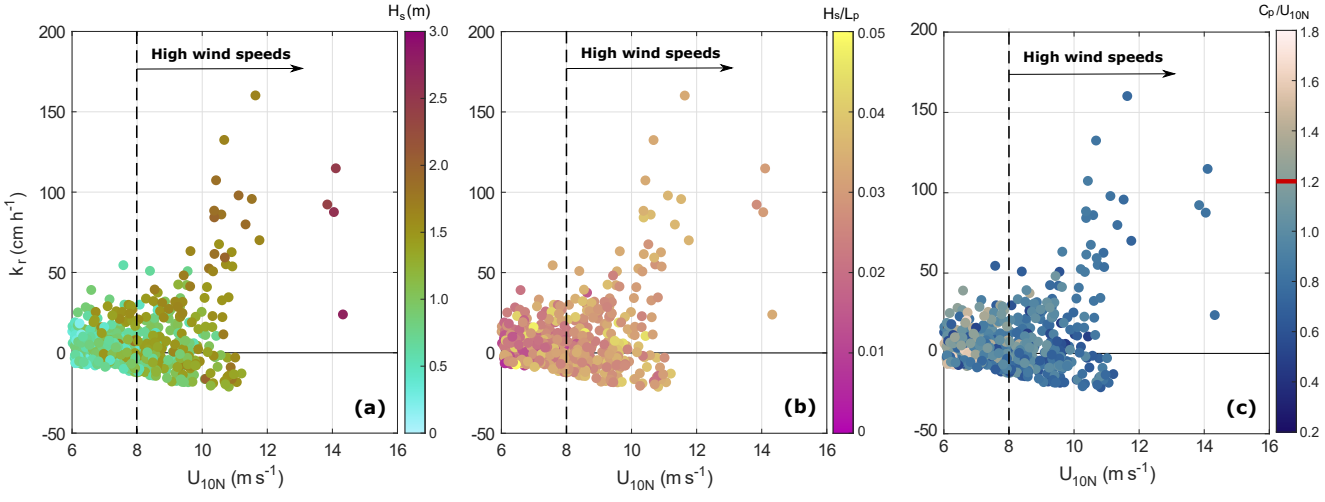

Figure 6. Residual gas transfer velocity ($k_r = k_{660} - k_{W14}$) as a function of the 10 m neutral wind speed under high wind speed conditions. The color represents a) significant wave height, b) wave steepness (H_s/L_p), and c) wave age (C_p/U_{10N}). The vertical dashed lines mark the threshold between intermediate ($6 < U_{10N} < 8\,\mathrm{m\,s^{-1}}$) and high ($U_{10N} > 8\,\mathrm{m\,s^{-1}}$) wind speeds. The red mark in c) indicates the theoretical threshold between wind sea (C_p/U_{10N} <1.2) and swell (C_p/U_{10N} >1.2).

https://doi.org/10.5194/bg-2022-82
Preprint. Discussion started: 30 March 2022

Biogeosciences Discussions Open Access EGU

based parametrization. While, moderate negative values of ΔpCO_2 occurred for both positive and negative k_r values. At these relatively high wind-speed conditions (U_{10N} >8 m s^{-1}), the water column was well mixed and, while some scatter is observed, the largest values of k_r were associated with a deep mixed layer (Fig. 7b). Relatively shallow MLD values remained closer to the $k_r = 0$ line and below it. The combined effect of ΔpCO_2 and MLD, was strongly modulated by seasonal patterns. During the winter, strong and persistent vertical mixing occurred along with positive ΔpCO_2 (Fig. 3a). During the summer, shallower MLD and negative ΔpCO_2 were observed.

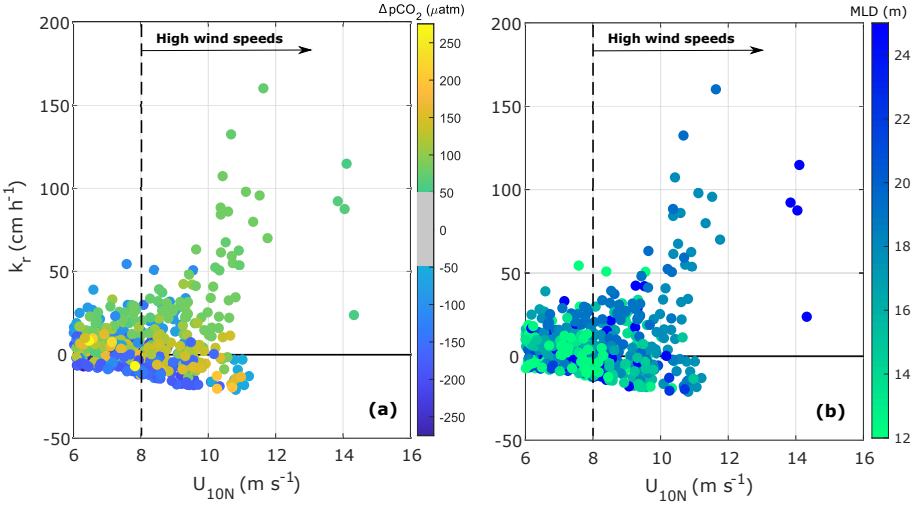

Figure 7. Residual gas transfer velocity ($k_r = k_{660} - k_{W14}$) as a function of the 10 m neutral wind speed under high wind speed conditions. The color represents a) the ΔpCO_2, and b) the mixed layer depth (MLD). The vertical dashed lines mark the threshold between intermediate ($6 < U_{10N} < 8\,\mathrm{m\,s^{-1}}$) and high ($U_{10N} > 8\,\mathrm{m\,s^{-1}}$) wind speeds.

Atmospheric conditions such as atmospheric stability, relative humidity, and the total enthalpy flux seemed to be linked to the gas exchange efficiency as well (Fig. 8). In terms of the atmospheric stability, the differences between unstable, neutral, and stable conditions became evident at the highest wind speeds (Fig. 8a). An increased wind-speed dependency of k_{660} (and therefore of k_r) was observed under unstable conditions for wind speeds higher than 8 m s^{-1}. While k_r remained close to zero up to 10 m s^{-1} during stable and neutral conditions. At wind speeds higher than 10 m s^{-1}, k_r tended to decrease with wind speed during stable conditions, and to a lesser extent under neutral conditions. Furthermore, high k_r values were observed when high enthalpy fluxes occurred; meanwhile, the lowest values of the enthalpy flux were associated to negative k_r values (Fig. 8b). The relative humidity seemed to also play a role, with high RH values associated to negative k_r for wind speeds higher than 10 m s^{-1}. On the contrary, low RH were observed mostly during positive k_r (Fig. 8c). Some low RH values linked to negative k_r were observed at wind speeds higher that 10 m s^{-1}, however, these values were also related to close-to-zero values of the enthalpy flux. According to the results in Fig. 8, dry air during unstable atmospheric conditions was not only associated to large enthalpy fluxes, but it also triggered a significant increase in the efficiency of the gas exchange.

https://doi.org/10.5194/bg-2022-82
Preprint. Discussion started: 30 March 2022

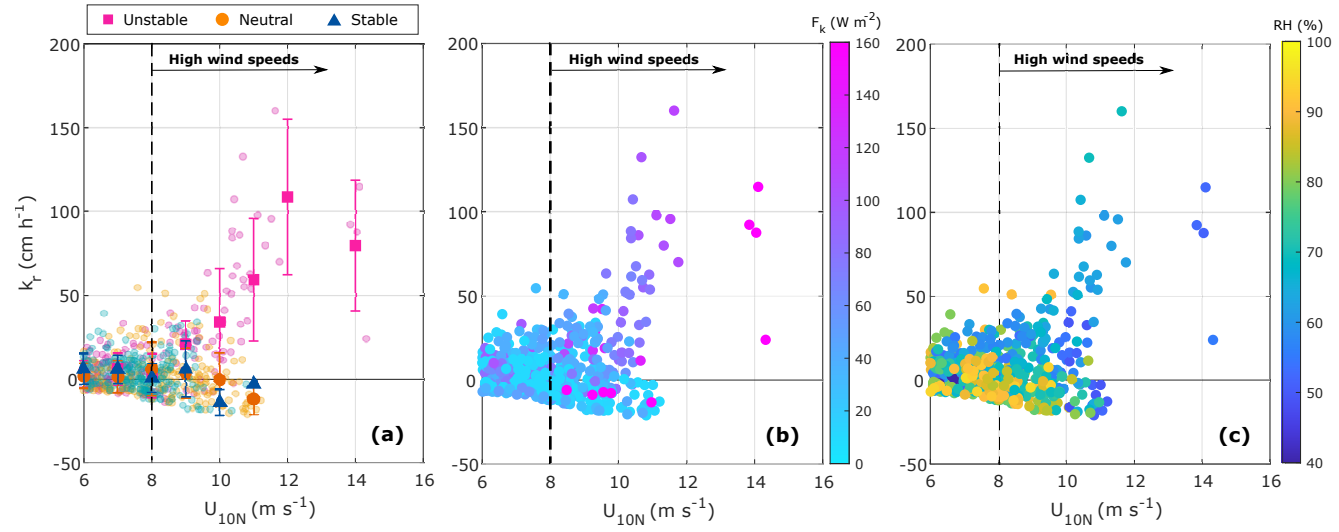

Figure 8. Residual gas transfer velocity ($k_r = k_{660} - k_{W14}$) as a function of the 10 m neutral wind speed under high wind speed conditions. The color represents a) atmospheric stability, b) enthalpy flux, and c) relative humidity. In a) the filled symbols represent the bin average under each atmospheric regime and the bars indicate $\pm 1\sigma$. The vertical dashed lines mark the threshold between intermediate ($6 < U_{10N} < 8\,\mathrm{m\,s^{-1}}$) and high ($U_{10N} > 8\,\mathrm{m\,s^{-1}}$) wind speeds.

3.2.2 Controls on k_{660} under low wind-speed conditions

Under low wind-speed conditions ($U_{10N} \leq 6\,\mathrm{m\,s^{-1}}$) the wave field showed smaller (H_s<1 m) and less steep waves (Fig. 9a and b). Under these conditions, the waves tended to be older (C_p/U_{10N}>1.2, Fig. 9c), indicating a larger proportion of swell waves in comparison to the locally generated waves observed at higher wind speeds. The characteristics of the wave field did not show a clear relation with the behaviour of k_r. Furthermore, the analysis of other water-side parameters such as ΔpCO_2, MLD, and water-side convection helped explain part of the variability in the gas transfer velocity (Fig. 10). The largest ΔpCO_2 values, with absolute magnitudes higher than 200 μatm, were observed within ± 10 μatm of the horizontal line, i.e. $k_r \approx 0$ (Fig. 10a). Positive ΔpCO_2 corresponded to positive k_r, while strong negative values of ΔpCO_2 were mostly associated with negative k_r for wind speeds below $6\,\mathrm{m\,s^{-1}}$, but a large scatter is observed. Under these calm wind speed conditions, the values of MLD were generally low, with the lowest (MLD<15) values showing a larger scatter (Fig. 10b). The pattern of ΔpCO_2 and MLD was associated with the seasonal cycles, suggesting that shallow MLD typical of the summer months may hinder the downward transport of CO_2 into the sea. In addition to ΔpCO_2 and the MLD, water-side convection was a relevant parameter under unstable atmospheric conditions (Fig. 10c). Low values of the water-side convective scale (w^*), as defined in Rutgersson and Smedman (2010), were observed on and below the horizontal line (i.e. $k_r \approx 0$). Meanwhile, some of the scattered data could be associated with larger values of the water-side convective scale ($w^* > 0.01\,\mathrm{m\,s^{-1}}$). Water-side convection seemed to be particularly relevant for positive fluxes, which occurred during the winter when $\Delta T > 0$ (Fig. 4c) indicating cooling of the surface. The rest of the scattered data which occurred during negative ΔpCO_2 and shallow MLD (Fig. 10a and 10b)

https://doi.org/10.5194/bg-2022-82
Preprint. Discussion started: 30 March 2022

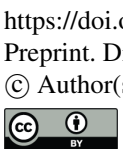

Biogeosciences Discussions Open Access EGU

cannot be explained by water-side convection or any other parameter assessed in this study. Furthermore, the interpretation of these data should be taken with some caution as the strong stratification, relatively weak ΔpCO_2, and the possibility of strong heterogeneity in terms of the biogeochemical properties might hinder our capacity to calculate k_{660} from pCO_2^w and FCO_2. Under neutral and stable atmospheric conditions, water-side convection is not a relevant mechanisms (Rutgersson and Smedman, 2010; Rutgersson et al., 2011; Norman et al., 2013b). At low wind speed conditions, atmospheric controls (not shown) did not play any significant role on the gas exchange.

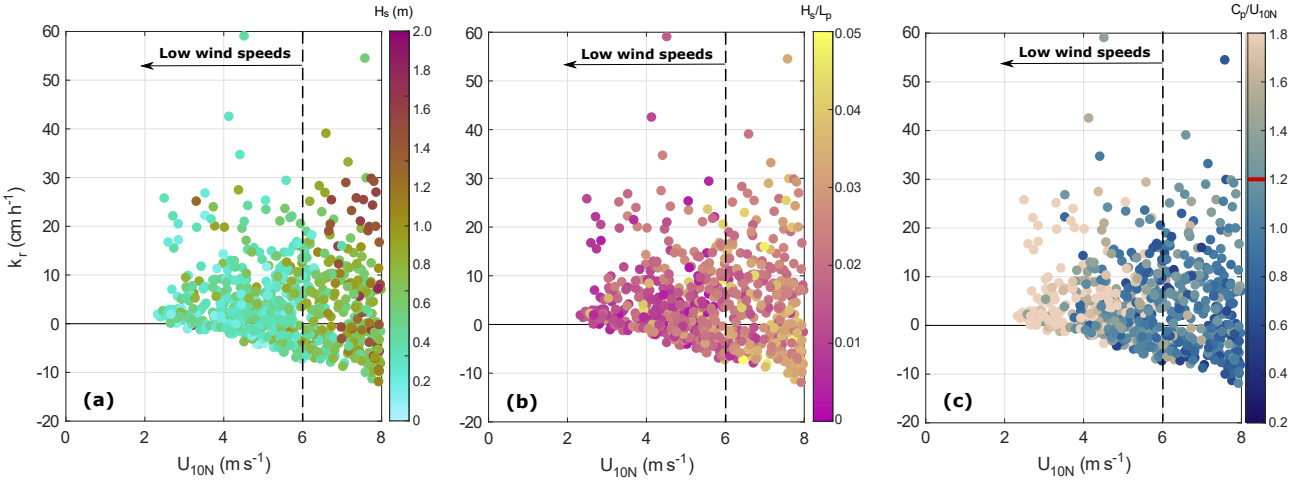

Figure 9. Residual gas transfer velocity ($k_r = k_{660} - k_{W14}$) as a function of the 10 m neutral wind speed under low wind speed conditions. The color represents a) significant wave height, b) wave steepness (H_s/L_p), and c) wave age (C_p/U_{10N}). The vertical dashed lines mark the threshold between low ($U_{10N} < 6\,\mathrm{m\,s^{-1}}$) and intermediate ($6 < U_{10N} < 8\,\mathrm{m\,s^{-1}}$) wind speeds. The red mark in c) indicates the theoretical threshold between wind sea (C_p/U_{10N} <1.2) and swell (C_p/U_{10N} >1.2).

3.2.3 Controls on k_{660} in the transition range

Wind speeds between 6 and 8 $\mathrm{m\,s^{-1}}$ were considered here as the transition range between low and high wind speeds. For convenience, the results of this transition range were included in the figures of both high and low wind speed conditions (Sect. 3.2.1 and Sect. 3.2.2, respectively). During the transition range, the atmospheric controls did not seem to be relevant (similar to low wind-speed conditions). Furthermore, the water-side mechanisms showed a mixed behaviour. The wave field showed waves with an average H_s of 0.9 m, in comparison to the 1.4 and 0.6 m of the high and low wind speed regimes, respectively. However, wave steepness and wave age at intermediate winds showed average values of H_s/L_p=0.03 and C_p/U_{10N}=1.1 similar to the mean values of H_s/L_p=0.03 and C_p/U_{10N}=1.0 observed at higher wind speeds. Both the wave field and the wind speed seemed to cause stronger mixing as larger values of MLD reaching the entire water column (ca 25 m) were observed under the transition range in contrast to the more persistent stratification at lower wind speeds (Fig. 10b). Values of MLD during these intermediate wind speeds were still lower, on average, than those observed during the high wind speed regime. Meanwhile,

https://doi.org/10.5194/bg-2022-82
Preprint. Discussion started: 30 March 2022

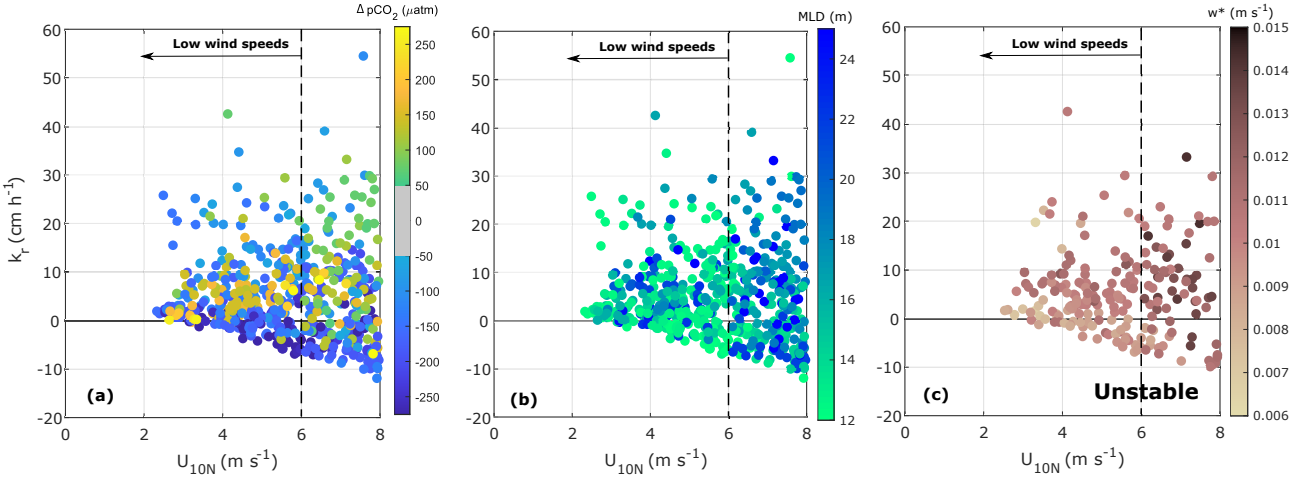

Figure 10. Residual gas transfer velocity ($k_r = k_{660} - k_{W14}$) as a function of the 10 m neutral wind speed under low wind speed conditions. The color represents a) the ΔpCO_2, b) the mixed layer depth (MLD), and c) the water-side convective scale (w^*) as defined in Rutgersson and Smedman (2010), during unstable atmospheric conditions. The vertical dashed lines mark the threshold between low ($U_{10N} < 6\,\mathrm{m\,s^{-1}}$) and intermediate ($6 < U_{10N} < 8\,\mathrm{m\,s^{-1}}$) wind speeds.

large values of w^* suggest the mixing caused by water-side convective processes during unstable atmospheric conditions might be relevant at the intermediate wind speeds (Fig. 10c). In terms of the thermodynamic forcing, positive values of ΔpCO_2 were associated to positive values of k_r similar to the behaviour at lower wind speeds. However, the increased mixing observed at intermediate winds seemed to also enhance fluxes during moderately positive ΔpCO_2, similar to the observed pattern during high wind speed conditions (Fig. 7a).

4 Discussion

We used nine years of eddy-covariance-based FCO_2 data to evaluate the effect of different control mechanisms on air–sea CO_2 gas exchange. By using this long record, we were able to capture the seasonal variability of the FCO_2 and other parameters relevant to the gas exchange (Sect. 3.1), as well as directly assess controls on k_{660} (Sect. 3.2). The empirically derived k_{660} values showed, in general, a similar wind-speed dependency as the two wind-based parametrizations, the quadratic relationship from Wanninkhof (2014), and the cubic relationship from McGillis et al. (2001). These parametrizations were used as references and we considered that using other commonly-used parametrizations (e.g. Wanninkhof and McGillis, 1999; Nightingale et al., 2000; Ho et al., 2006) would show similar results. However, the scatter of the data suggested that a large proportion of the variability in k_{660} was not explained by variations in the wind speed (Fig. 5). Mechanisms other than the wind have been recognized to be relevant controls on air–sea gas exchange processes, particularly in heterogeneous environments such as marginal and coastal seas (e.g. Upstill-Goddard, 2006; Gutiérrez-Loza et al., 2021). Based on the results presented here, we showed that wind-based parameterizations developed for larger basins and open-ocean conditions can be adequate approxima-

https://doi.org/10.5194/bg-2022-82
Preprint. Discussion started: 30 March 2022

tions for long-term gas transfer velocity calculations, even in heterogeneous environments such as the studied area. However, we noticed conditions where the existing models failed to replicate the observations, and we further showed that in order to capture the short-term variability in k_{660} additional process need to be accounted for.

The characteristics of the wave field are one of the most important parameters involved on the air–sea gas transfer directly affecting the conditions of the interface. However, the effect of waves on gas exchange has been very seldom studied in coastal regions (e.g. Gutiérrez-Loza et al., 2018). We analyzed different parameters describing the wave field (significant wave height, wave steepness, and wave age) and their effect on the gas transfer velocity. At high wind speeds, the waves were found to be locally generated by the wind (i.e. wind sea), which made it hard to separate the effect of the waves from that of the wind. The wave climate in the Baltic Sea is characterized by predominant short wind sea and scarce long swell (Soomere, 2022). Furthermore, the effect of swell waves was not relevant at high wind speed conditions, and while at lower wind speeds some effect from swell could be expected, such effect was partly excluded here as wind speeds lower than $2\,\mathrm{m\,s^{-1}}$ were removed from the analysis. Values of wave steepness suggested that there was no systematic wave breaking. However, empirical knowledge of the study site suggests the presence of breaking, particularly of the smallest/youngest waves. These waves are not expected to generate significant bubble entrainment into the upper layer of the sea, but generation of sea spray is expected at the highest wind speeds.

The effect of sea spray in the air–sea gas exchange has been reported before (Andreas et al., 2016, 2017). However, the impact of a broken surface caused by wave breaking and whitecaping, has been shown to cause an asymmetric transport due to the injection of bubbles into the ocean enhancing the negative (downward) fluxes (Woolf, 1997; Leighton et al., 2018). This was not seen here, instead, we found that the increase in the k_{660} was associated to the ocean-to-atmosphere (upward) transport in what we suggest is the effect of sea spray. This effect was clearly affected with the seasonal variability as the increased k_{660} where observed during the winter months, when dry and cold air (colder than the ocean) are common (Fig.4c and e). During the winter months positive CO_2 gradients prevail and positive gas and heat fluxes are most often observed. Dedicated analysis of the effect of bubbles and sea spray in coastal regions are still necessary. Particularly at high latitudes, where strong seasonality may cause significant differences in the forcing mechanisms modulating the influx and eflux of gas into/from the ocean (see Sect. 3.1). A brief analysis of the effect of sea spray on air–sea fluxes made using a bulk algorithm for turbulent air–sea fluxes, freely available from www.nwra.com/resumes/andreas/software.php (Andreas et al., 2008). The results showed that the large enthalpy fluxes observed under unstable conditions at high wind speeds (Fig. 8b) can be attributed to sea spray. Figure 11 shows sea spray mediated fluxes of up to $30\,\mathrm{W\,m^{-2}}$ (up to 20 % of the total enthalpy flux) under these conditions. We suggest sea spray can enhance the transport of CO_2 across the interface, as it does with heat and moisture. Based on our results, this mechanism can be a relevant control of the gas exchange by enhancing upward CO_2 fluxes at wind speeds higher than 8–10 $\mathrm{m\,s^{-1}}$ under unstable atmospheric conditions and low relative humidity. Further data under these particular conditions is necessary to establish a better understanding of the effect of sea spray mediated gas fluxes.

Under calm wind speed conditions, with U_{10N}<6 $\mathrm{m\,s^{-1}}$, the effect of water-side convection was found to be relevant to explain the lager values of k_{660} during unstable atmospheric conditions at these wind speeds. Previous studies have shown the effect of convective processes on the gas transfer in the Baltic Sea (Rutgersson and Smedman, 2010; Norman et al., 2013b).

https://doi.org/10.5194/bg-2022-82
Preprint. Discussion started: 30 March 2022

Biogeosciences Discussions Open Access EGU

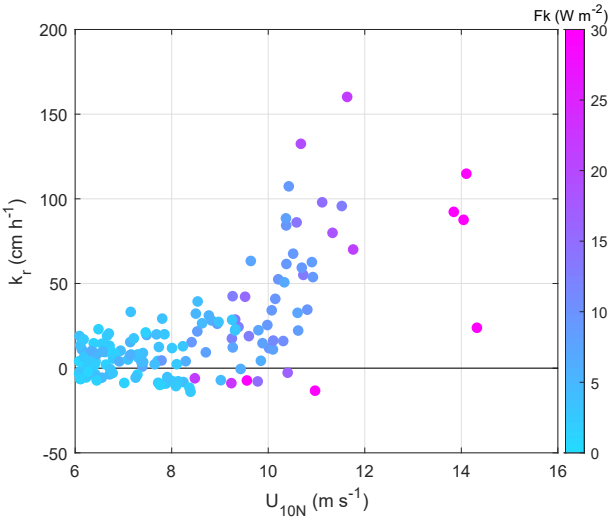

Figure 11. Residual gas transfer velocity ($k_r = k_{660} - k_{W14}$) as a function of the 10 m neutral wind speed under low wind speed conditions. The color represents the sea-spray-mediated enthalpy flux calculated using a bulk algorithm for air–sea turbulent fluxes (Andreas et al., 2008).

The same studies showed that the water-side convective processes are not relevant under stable and neutral conditions, as well as at wind speeds higher than $8\,\mathrm{m\,s^{-1}}$.

The ability to correctly calculate the gas transfer velocity from eddy covariance FCO_2 and ΔpCO_2 measurements is a matter of discussion. For the data presented here, this limitation was evident at low wind speeds during the summer months, when a strongly stratified and highly heterogeneous surface layer might not be well represented by the pCO_2^w measurements at 4 m depth. In order to avoid this uncertainty in our k_{660} calculations, we removed data based on a ΔT_w criterion (see Sect. 2.2). However, we still observed scattered data at the lowest wind speeds corresponding to moderate ΔpCO_2 negative values and shallow MLD (Fig. 10a and b). Due to the uncertainty, we did not make further conclusions based on these data, and we encourage the reader to be cautious when interpreting these results.

The occurrence of upwelling events can be up to 25-30% in some regions of the Baltic Sea (Lehmann et al., 2012). Norman et al. (2013a) found that effect of these events on the annual mean FCO_2 can reach up to 25% for the Baltic Sea conditions. In this study we did not analyze the relative importance of upwelling on FCO_2 or k_{660}, however, we recognize that part of the observed inter-annual variability might be caused by upwelling events. An in-depth analysis of the data is necessary to evaluate individual upwelling events captured during the nine years of measurements. Furthermore, using the parameterization suggested by Pereira et al. (2018) based on the skin temperature, we calculated a rough estimate of the effect of surfactants on our long-term k_{660}. The results suggest an overall effect of merely -0.1 %, suggesting a very small reduction of k_{660} when surfactants are taken into account. A detail analysis of the effect of surface films is beyond the scope of this study. Nevertheless, we recognize that this process might be particularly relevant in coastal seas and other shallow bodies of water. The analysis of the effect of sea ice, precipitation, Langmuir circulation, and other processes in the Baltic Sea is still pending.

https://doi.org/10.5194/bg-2022-82
Preprint. Discussion started: 30 March 2022

We presented what we believe is the longest record of directly measured FCO_2 and the corresponding gas transfer velocities from in situ data. Regardless of the length of our data set, we still found three major limitations when addressing the effect of forcing mechanisms on air–sea gas exchange: 1) the use of a land-based station provides significant advantages, but it hinders the evaluation of the spatial variability of the exchange; 2) the intrinsic characteristics of the eddy covariance technique, in combination to the exclusion of wind directions not representative of open-sea conditions, resulted in a patchy data set with significant gaps throughout the time series; and 3) limited amount of data at high wind speeds ($U_{10N} > 10\,\mathrm{m\,s^{-1}}$) was recorded, which hindered the analysis and increases the uncertainties at those critical wind conditions. The results presented here provide significant insights on the air–sea gas exchange and its variability. Nevertheless, the limitations are still large and a continued effort from the scientific community is required.

Global coastal oceans and marginal seas are one of the most vulnerable environments subjected to the effect of climate change and anthropogenic pressures (Pachauri et al., 2014). Understanding the role of these regions in the global carbon cycle has become an essential aspect in order to address the challenges of the current and future climates. In this sense, the Baltic Sea can be seen as a test basin which provides a wide variety of physical and biogeochemical conditions. At the same time, the carbon system of the Baltic Sea has been relatively well-documented (e.g. Kuliński and Pempkowiak, 2011; Schneider and Müller, 2018), and the region has been a relevant study area in terms of mitigation and environmental management (Reusch et al., 2018). The results presented here are most probably relevant for other marginal seas and coastal areas.

5 Conclusions

We presented a large data set of directly measured air–sea CO_2 fluxes by eddy covariance from a land-based station in the Baltic Sea. The forcing mechanisms acting on the surface of the ocean and their relative effect on the gas exchange can widely vary depending on the wind-speed. Therefore, the air–sea gas exchange, controlled by such forcing mechanisms, can also be expected to be affected in different ways depending on the wind-speed regime. We investigated the effect of the water-side and atmospheric conditions on the gas transfer velocity under relatively high, intermediate, and low wind speed regimes.

At high wind speeds larger values of the residual gas transfer velocity were observed. These values occurred during events of cold and dry air, under unstable atmospheric conditions. We suggest, based on these results, that sea spray might be one of the most effective mechanisms enhancing air–sea CO_2 fluxes under these conditions, most probably due to large evaporation rates. The effect of the wave field was particularly evident in terms of the significant wave height, with high gas transfer velocity values occurring when large values of H_s were observed. However, the effect of the wave field was not completely decoupled from the effect of the wind given that most of the waves were locally generated. Thus, theoretically removing the wind effect might not be sufficient to individually evaluate the effect of waves on the gas exchange. Intermediate wind speeds showed a mixed behaviour, thus, we defined these wind speeds as a transition range. Under these conditions, the mixing induced by the wind and waves to the upper layer of the sea was found to be the most relevant parameter for the gas exchange. Particularly when moderate ΔpCO_2 values occurred, similarly to high wind speed conditions. Under low wind speed conditions, water-side

https://doi.org/10.5194/bg-2022-82
Preprint. Discussion started: 30 March 2022

convection was the only parameter explaining part of the variability on k_r, particularly during the winter. During the summer, strong stratification occurred, hindering the downward fluxes.

Currently existing wind-based parametrizations showed to adequately represent k_{660} in the long-term averages. However, further investigation of parameters affecting the seasonal and inter-annual variability of the fluxes is needed to improve our understanding of air–sea gas exchange and adequately represent k_{660} in shorter time scales. Similarly, a detail analysis of bubble- and sea-spray-mediated fluxes is needed to contribute to the understanding of CO_2 fluxes in the coastal regions.

https://doi.org/10.5194/bg-2022-82
Preprint. Discussion started: 30 March 2022

Data availability. The raw data supporting the conclusions of this manuscript is available upon request.

Author contributions. LG-L, MW, ES and AR were involved in the conceptualization of the project. AR was in charge of the project administration and funding acquisition. The formal analysis was carried out by LG-L with the support of EN. LG-L, MW, EN and AR participated in the continuous maintenance of the Östergarnsholm station and data acquisition. LG-L wrote the original draft with contribution from all the co-authors.

Competing interests. The authors declare that they have no conflict of interest.

Acknowledgements. The ICOS station Östergarnsholm is funded by the Swedish Research Council (Vetenskapsrådet) grants 2012-03902 and 2013-02044, and Uppsala University. The wave data was provided by Heidi Pettersson from the Finish Meteorological Insitute (FMI) to whom the authors are grateful.

https://doi.org/10.5194/bg-2022-82
Preprint. Discussion started: 30 March 2022

References

Andreas, E., Vlahos, P., and Monahan, E.: The potential role of sea spray droplets in facilitating air-sea gas transfer, in: IOP conference series: earth and environmental science, vol. 35, p. 012003, IOP Publishing, 2016.

Andreas, E. L., Persson, P. O. G., and Hare, J. E.: A bulk turbulent air–sea flux algorithm for high-wind, spray conditions, Journal of Physical Oceanography, 38, 1581–1596, 2008.

Andreas, E. L., Vlahos, P., and Monahan, E. C.: Spray-mediated air-sea gas exchange: the governing time scales, Journal of Marine Science and Engineering, 5, 60, 2017.

Ashton, I. G., Shutler, J. D., Land, P. E., Woolf, D. K., and Quartly, G. D.: A sensitivity analysis of the impact of rain on regional and global sea–air fluxes of CO_2, PloS one, 11, 2016.

Aubinet, M., Vesala, T., and Papale, D.: Eddy covariance: a practical guide to measurement and data analysis, Springer Science & Business Media, 2012.

Baldocchi, D. D., Hincks, B. B., and Meyers, T. P.: Measuring biosphere–atmosphere exchanges of biologically related gases with micrometeorological methods, Ecology, 69, 1331–1340, 1988.

Barua, D. K.: Beaufort wind scale, Encyclopedia of Coastal Science. Dordrecht: Springer Netherlands, 2005.

Bell, T. G., Landwehr, S., Miller, S. D., De Bruyn, W. J., Callaghan, A. H., Scanlon, B., Ward, B., Yang, M., and Saltzman, E. S.: Estimation of bubble-mediated air–sea gas exchange from concurrent DMS and CO_2 transfer velocities at intermediate–high wind speeds, Atmospheric Chemistry and Physics, 17, 9019–9033, 2017.

Blomquist, B., Brumer, S., Fairall, C., Huebert, B., Zappa, C., Brooks, I., Yang, M., Bariteau, L., Prytherch, J., Hare, J., et al.: Wind speed and sea state dependencies of air–sea gas transfer: Results from the High Wind speed Gas exchange Study (HiWinGS), Journal of Geophysical Research: Oceans, 122, 8034–8062, 2017.

Borges, A. V., Delille, B., and Frankignoulle, M.: Budgeting sinks and sources of CO_2 in the coastal ocean: Diversity of ecosystems count, Geophysical Research Letters, 32, L14 601, 2005.

Brumer, S. E., Zappa, C. J., Blomquist, B. W., Fairall, C. W., Cifuentes-Lorenzen, A., Edson, J. B., Brooks, I. M., and Huebert, B. J.: Wave-related Reynolds number parameterizations of CO_2 and DMS transfer velocities, Geophysical Research Letters, 44, 9865–9875, 2017.

Chen, C.-T. A., Huang, T.-H., Chen, Y.-C., Bai, Y., He, X., and Kang, Y.: Air–sea exchanges of CO_2 in the world's coastal seas, Biogeosciences, 10, 2013.

Ciais, P., Sabine, C., Bala, G., Bopp, L., Brovkin, V., Canadell, J., Chhabra, A., DeFries, R., Galloway, J., Heimann, M., et al.: Carbon and other biogeochemical cycles, in: Climate change 2013: the physical science basis. Contribution of Working Group I to the Fifth Assessment Report of the Intergovernmental Panel on Climate Change, edited by Stocker, T., Qin, D., Plattner, G.-K., Tignor, M., Allen, S., Boschung, J., Nauels, A., Xia, Y., Bex, V., and Midgley, P., pp. 465–570, Cambridge University Press, 2013.

Erickson III, D. J.: A stability dependent theory for air-sea gas exchange, Journal of Geophysical Research: Oceans, 98, 8471–8488, 1993.

Friedlingstein, P., Jones, M. W., O'Sullivan, M., Andrew, R. M., Bakker, D. C. E., Hauck, J., Le Quéré, C., Peters, G. P., Peters, W., Pongratz, J., et al.: Global Carbon Budget 2021, Earth System Science Data Discussions, 2021, 1–191, https://doi.org/10.5194/essd-2021-386, 2021.

Gutiérrez-Loza, L., Ocampo-Torres, F. J., and García-Nava, H.: The Effect of Breaking Waves on CO_2 Air–Sea Fluxes in the Coastal Zone, Boundary-Layer Meteorology, 168, 343–360, 2018.

https://doi.org/10.5194/bg-2022-82
Preprint. Discussion started: 30 March 2022

Gutiérrez-Loza, L., Wallin, M. B., Sahlée, E., Holding, T., Shutler, J. D., Rehder, G., and Rutgersson, A.: Air–sea CO2 exchange in the Baltic Sea—A sensitivity analysis of the gas transfer velocity, Journal of Marine Systems, 222, 103 603, 2021.

Ho, D. T., Law, C. S., Smith, M. J., Schlosser, P., Harvey, M., and Hill, P.: Measurements of air–sea gas exchange at high wind speeds in the Southern Ocean: Implications for global parameterizations, Geophysical Research Letters, 33, 2006.

Högström, U., Sahlée, E., Drennan, W. M., Kahma, K. K., Smedman, A.-S., Johansson, C., Pettersson, H., Rutgersson, A., Tuomi, L., Zhang, F., and Johansson, M.: Momentum fluxes and wind gradients in the marine boundary layer: A multi platform study, Boreal environment research, 13, 475–502, 2008.

Honkanen, M., Müller, J. D., Seppälä, J., Rehder, G., Kielosto, S., Ylöstalo, P., Mäkelä, T., Hatakka, J., and Laakso, L.: The diurnal cycle of pCO_2 in the coastal region of the Baltic Sea, Ocean Science, 17, 1657–1675, 2021.

Jacobs, E., Bittig, H. C., Gräwe, U., Graves, C. A., Glockzin, M., Müller, J. D., Schneider, B., and Rehder, G.: Upwelling-induced trace gas dynamics in the Baltic Sea inferred from 8 years of autonomous measurements on a ship of opportunity, Biogeosciences, 18, 2679–2709, 2021.

Jessup, A., Zappa, C. J., and Yeh, H.: Defining and quantifying microscale wave breaking with infrared imagery, Journal of Geophysical Research: Oceans, 102, 23 145–23 153, 1997.

Kaimal, J. C. and Finnigan, J. J.: Atmospheric boundary layer flows: their structure and measurement, Oxford university press, 1994.

Kljun, N., Calanca, P., Rotach, M., and Schmid, H. P.: A simple two-dimensional parameterisation for Flux Footprint Prediction (FFP), Geoscientific Model Development, 8, 3695–3713, 2015.

Kuliński, K. and Pempkowiak, J.: The carbon budget of the Baltic Sea, Biogeosciences, 8, 3219–3230, 2011.

Laruelle, G. G., Dürr, H. H., Slomp, C. P., and Borges, A. V.: Evaluation of sinks and sources of CO_2 in the global coastal ocean using a spatially-explicit typology of estuaries and continental shelves, Geophysical Research Letters, 37, 2010.

Laruelle, G. G., Lauerwald, R., Pfeil, B., and Regnier, P.: Regionalized global budget of the CO_2 exchange at the air-water interface in continental shelf seas, Global biogeochemical cycles, 28, 1199–1214, 2014.

Lehmann, A., Myrberg, K., and Höflich, K.: A statistical approach to coastal upwelling in the Baltic Sea based on the analysis of satellite data for 1990–2009, Oceanologia, 54, 369–393, 2012.

Leighton, T. G., Coles, D. G., Srokosz, M., White, P. R., and Woolf, D. K.: Asymmetric transfer of CO_2 across a broken sea surface, Scientific reports, 8, 1–9, 2018.

Löffler, A., Schneider, B., Perttilä, M., and Rehder, G.: Air–sea CO_2 exchange in the Gulf of Bothnia, Baltic Sea, Continental Shelf Research, 37, 46–56, 2012.

McGillis, W. R., Edson, J. B., Hare, J. E., and Fairall, C. W.: Direct covariance air–sea CO_2 fluxes, J. Geophys. Res.-Oceans, 106, 16 729–16 745, 2001.

Nightingale, P. D., Malin, G., Law, C. S., Watson, A. J., Liss, P. S., Liddicoat, M. I., Boutin, J., and Upstill-Goddard, R. C.: In situ evaluation of air–sea gas exchange parameterizations using novel conservative and volatile tracers, Global Biogeochemical Cycles, 14, 373–387, 2000.

Nilsson, E., Bergström, H., Rutgersson, A., Podgrajsek, E., Wallin, M. B., Bergström, G., Dellwik, E., Landwehr, S., and Ward, B.: Evaluating humidity and sea salt disturbances on CO_2 flux measurements, Journal of Atmospheric and Oceanic Technology, 35, 859–875, 2018.

Norman, M., Parampil, S. R., Rutgersson, A., and Sahlée, E.: Influence of coastal upwelling on the air–sea gas exchange of CO_2 in a Baltic Sea Basin, Tellus B: Chemical and Physical Meteorology, 65, 21 831, 2013a.

https://doi.org/10.5194/bg-2022-82
Preprint. Discussion started: 30 March 2022

Norman, M., Rutgersson, A., and Sahlée, E.: Impact of improved air–sea gas transfer velocity on fluxes and water chemistry in a Baltic Sea model, Journal of Marine Systems, 111, 175–188, 2013b.

Pachauri, R. K., Allen, M. R., Barros, V. R., Broome, J., Cramer, W., Christ, R., Church, J. A., Clarke, L., Dahe, Q., Dasgupta, P., et al.: Climate change 2014: synthesis report. Contribution of Working Groups I, II and III to the fifth assessment report of the Intergovernmental Panel on Climate Change, Ipcc, 2014.

Parard, G., Rutgersson, A., Parampil, S. R., and Charantonis, A. A.: The potential of using remote sensing data to estimate air–sea CO_2 exchange in the Baltic Sea, Earth System Dynamics, 8, 1093–1106, 2017.

Pereira, R., Ashton, I., Sabbaghzadeh, B., Shutler, J. D., and Upstill-Goddard, R. C.: Reduced air–sea CO2 exchange in the Atlantic Ocean due to biological surfactants, Nature Geoscience, 11, 492–496, 2018.

Reusch, T. B., Dierking, J., Andersson, H. C., Bonsdorff, E., Carstensen, J., Casini, M., Czajkowski, M., Hasler, B., Hinsby, K., Hyytiäinen, K., et al.: The Baltic Sea as a time machine for the future coastal ocean, Science Advances, 4, 2018.

Ribas-Ribas, M., Helleis, F., Rahlff, J., and Wurl, O.: Air–Sea CO_2 exchange in a large annular wind-wave tank and the effects of surfactants, Frontiers in Marine Science, p. 457, 2018.

Roobaert, A., Laruelle, G. G., Landschützer, P., Gruber, N., Chou, L., and Regnier, P.: The Spatiotemporal Dynamics of the Sources and Sinks of CO_2 in the Global Coastal Ocean, Global Biogeochemical Cycles, 33, 1693–1714, https://doi.org/https://doi.org/10.1029/2019GB006239, 2019.

Rutgersson, A. and Smedman, A. S.: Enhanced air–sea CO_2 transfer due to water-side convection, Journal of Marine systems, 80, 125–134, 2010.

Rutgersson, A., Smedman, A.-S., and Omstedt, A.: Measured and simulated latent and sensible heat fluxes at two marine sites in the Baltic Sea, Boundary-Layer Meteorology, 99, 53–84, 2001.

Rutgersson, A., Norman, M., Schneider, B., Pettersson, H., and Sahlée, E.: The annual cycle of carbon dioxide and parameters influencing the air–sea carbon exchange in the Baltic Proper, Journal of Marine Systems, 74, 381–394, https://doi.org/10.1016/j.jmarsys.2008.02.005, 2008.

Rutgersson, A., Norman, M., and Åström, G.: Atmospheric CO_2 variation over the Baltic Sea and the impact on air–sea exchange, Boreal environment research, 14, 238–249, 2009.

Rutgersson, A., Smedman, A., and Sahlée, E.: Oceanic convective mixing and the impact on air–sea gas transfer velocity, Geophysical Research Letters, 38, 2011.

Rutgersson, A., Pettersson, H., Nilsson, E., Bergström, H., Wallin, M. B., Nilsson, E. D., Sahlée, E., Wu, L., and Mårtensson, E. M.: Using land-based stations for air–sea interaction studies, Tellus A: Dynamic Meteorology and Oceanography, 72, 1–23, 2020.

Sahlée, E., Smedman, A. S., Rutgersson, A., and Högström, U.: Spectra of CO_2 and water vapour in the marine atmospheric surface layer, Boundary-layer meteorology, 126, 279–295, 2008.

Schneider, B. and Müller, J. D.: Biogeochemical transformations in the Baltic Sea, Springer, 2018.

Schneider, B., Gülzow, W., Sadkowiak, B., and Rehder, G.: Detecting sinks and sources of CO_2 and CH_4 by ferrybox-based measurements in the Baltic Sea: Three case studies, Journal of Marine Systems, 140, 13–25, 2014.

Sjöblom, A. and Smedman, A.-S.: The turbulent kinetic energy budget in the marine atmospheric surface layer, Journal of Geophysical Research: Oceans, 107, 6–1, 2002.

Smedman, A.-S., Högström, U., Bergström, H., Rutgersson, A., Kahma, K. K., and Pettersson, H.: A case study of air–sea interaction during swell conditions, Journal of Geophysical Research: Oceans, 104, 25 833–25 851, 1999.

https://doi.org/10.5194/bg-2022-82
Preprint. Discussion started: 30 March 2022

Soloviev, A. and Lukas, R.: The near-surface layer of the ocean: structure, dynamics and applications, vol. 48, Springer Science & Business Media, 2013.

Soomere, T.: Numerical simulations of wave climate in the Baltic Sea: a review, Oceanologia, 2022.

Stokes, G. G.: Supplement to a paper on the theory of oscillatory waves, Mathematical and Physical papers, 1, 18, 1880.

Takahashi, T., Sutherland, S. C., Wanninkhof, R., Sweeney, C., Feely, R. A., Chipman, D. W., Hales, B., Friederich, G., Chavez, F., Sabine, C., et al.: Climatological mean and decadal change in surface ocean pCO_2, and net sea–air CO_2 flux over the global oceans, Deep Sea Research Part II: Topical Studies in Oceanography, 56, 554–577, 2009.

Thomas, H. and Schneider, B.: The seasonal cycle of carbon dioxide in Baltic Sea surface waters, Journal of Marine Systems, 22, 53–67, 1999.

Thomas, H., Pempkowiak, J., Wulff, F., and Nagel, K.: The Baltic Sea, in: Carbon and nutrient fluxes in continental margins, pp. 334–346, Springer, 2010.

Thorpe, S., Osborn, T., Farmer, D., and Vagle, S.: Bubble clouds and Langmuir circulation: Observations and models, Journal of Physical Oceanography, 33, 2013–2031, 2003.

Upstill-Goddard, R. C.: Air–sea gas exchange in the coastal zone, Estuarine, Coastal and Shelf Science, 70, 388–404, 2006.

Von Schuckmann, K., Le Traon, P.-Y., Alvarez-Fanjul, E., Axell, L., Balmaseda, M., Breivik, L.-A., Brewin, R. J. W., Bricaud, C., Drevillon, M., Drillet, Y., et al.: The copernicus marine environment monitoring service ocean state report, Journal of Operational Oceanography, 9, s235–s320, 2016.

Wanninkhof, R.: Relationship between wind speed and gas exchange over the ocean revisited, Limnol. Oceanogr.- Meth., 12, 351–362, 2014.

Wanninkhof, R. and McGillis, W. R.: A cubic relationship between air–sea CO_2 exchange and wind speed, Geophysical Research Letters, 26, 1889–1892, 1999.

Webb, E. K., Pearman, G. I., and Leuning, R.: Correction of flux measurements for density effects due to heat and water vapour transfer, Quarterly Journal of the Royal Meteorological Society, 106, 85–100, 1980.

Weiss, R.: Carbon dioxide in water and seawater: the solubility of a non-ideal gas, Marine chemistry, 2, 203–215, 1974.

Woolf, D. K.: Bubbles and the air-sea transfer velocity of gases, Atmosphere-Ocean, 31, 517–540, 1993.

Woolf, D. K.: Bubbles and their role in gas exchange, p. 173–206, Cambridge University Press, 1997.

Woolf, D. K., Shutler, J. D., Goddijn-Murphy, L., Watson, A. J., Chapron, B., Nightingale, P. D., Donlon, C. J., Piskozub, J., Yelland, M. J., Ashton, I., et al.: Key uncertainties in the recent air–sea flux of CO_2, Global Biogeochemical Cycles, 2019.

Zhao, D., Toba, Y., Suzuki, Y., and Komori, S.: Effect of wind waves on air–sea gas exchange: Proposal of an overall CO_2 transfer velocity formula as a function of breaking-wave parameter, Tellus B: Chemical and Physical Meteorology, 55, 478–487, 2003.